CHEMISTRY OF MATERIALS
Article

Chem. Mater. **2011,** *23,* 301–308 301
DOI:10.1021/cm102472h

Shell Thickness Control of Nanoparticle/Polymer Assembled Microcapsules

Hitesh G. Bagaria,[†] Shyam B. Kadali,[†] and Michael S. Wong*[,†,‡]

[†]*Department of Chemical and Biomolecular Engineering and* [‡]*Department of Chemistry, Rice University, Houston, Texas 77005, United States*

Received August 28, 2010. Revised Manuscript Received December 6, 2010

Organic/inorganic composite microcapsules can be produced in water through a two-step charge-driven assembly of polyallylamine, citrate anions, and 13 nm silica nanoparticles. The shell is composed of nanoparticles intermixed with polymer, and is thick enough (100s of nm) to provide structural stability before or after drying. Controlling shell thickness, however, is currently difficult to perform. Presented here is a new method in which the shell wall can be thickened by contacting the as-synthesized capsules with silicic acid. This shell thickening was observed and quantified for a moderately broad, unimodal size distribution of capsular particles, through a combination of transmission electron and confocal fluorescence microscopies. Thermogravimetric analysis confirmed the deposition of additional silica, and Coulter counter measurements showed the mean capsule diameter of $\sim 4.5 \pm 2.2\ \mu$m changed negligibly with silicic acid treatment. The shell-thickening process occurred in an inward direction, in which the nanosized silicic acid oligomers most likely diffused through the permeable capsule wall and deposited within the wall and on the inner shell wall surface. Adjustable shell wall thicknesses in hybrid microcapsules provide enhanced capability for chemical encapsulation, storage, and release applications.

1. Introduction

Inorganic microcapsules that presently find applications as encapsulants in cosmetics[1] and as low-density high-strength fillers[2] have paved the way for more sophisticated organic−inorganic composite capsules.[3−5] Substituting the inorganic shell with an inorganic/polymer composite significantly increases the functionality of capsules that can potentially find wide ranging applications in medicine,[6,7] energy[8] and catalysis.[9,10]

The most extensively reported method on the synthesis of composite capsules is the layer-by-layer (LbL) assembly technique.[7,11,12] Some of the advantages of this method are the ability to form capsules with a variety of materials like inorganic nanoparticles, easy control of capsule size, and the ability to control shell thickness. On the other hand, the LbL technique suffers from the multiple processing steps needed in forming capsules, and the inconvenient requirement of sacrificial core removal through chemical etching (e.g., hydrofluoric acid for silica core). Although LbL assembly provides for model capsule materials, other methods that minimize the number of processing steps and do not require a sacrificial core would be more appealing for large-scale production of capsules.[13−15]

*Corresponding author. E-mail: mswong@rice.edu.

(1) Sol-Gel Technologies. http://www.sol-gel.com/.
(2) 3M Glass Bubbles. http://solutions.3m.com/wps/portal/3M/en_US/Energy-Advanced/Materials/Product_Info/Prod_Catalog-SMD/?nid=CR1NGJJX5QbeWHB23F5LMRgl (3/31/2009),
(3) Shchukin, D. G.; Sukhorukov, G. B.; Mohwald, H. Smart inorganic/organic nanocomposite hollow microcapsules. *Angew. Chem., Int. Ed.* **2003**, *42*(37), 4472–4475.
(4) Katagiri, K.; Koumoto, K.; Iseya, S.; Sakai, M.; Matsuda, A.; Caruso, F. Tunable UV-Responsive Organic-Inorganic Hybrid Capsules. *Chem. Mater.* **2009**, *21*(2), 195–197.
(5) Peyratout, C. S.; Dahne, L. Tailor-made polyelectrolyte microcapsules: From multilayers to smart containers. *Angew. Chem., Int. Ed.* **2004**, *43*(29), 3762–3783.
(6) Rivera Gil, P.; del Mercato, L. L.; del-Pino, P.; Munoz-Javier, A.; Parak, W. J. Nanoparticle-modified polyelectrolyte capsules. *Nano Today* **2008**, *3*(3−4), 12–21.
(7) De Geest, B. G.; De Koker, S.; Sukhorukov, G. B.; Kreft, O.; Parak, W. J.; Skirtach, A. G.; Demeester, J.; De Smedt, S. C.; Hennink, W. E. Polyelectrolyte microcapsules for biomedical applications. *Soft Matter* **2009**, *5*(2), 282–291.
(8) Lou, X. W.; Deng, D.; Lee, J. Y.; Archer, L. A. Preparation of SnO2/Carbon Composite Hollow Spheres and Their Lithium Storage Properties. *Chem. Mater.* **2008**, *20*(20), 6562–6566.
(9) Shenhar, R.; Norsten, T. B.; Rotello, V. M. Polymer-mediated nanoparticle assembly: Structural control and applications. *Adv. Mater.* **2005**, *17*(6), 657–669.
(10) Amali, A. J.; Rana, R. K. Trapping Pd(0) in nanoparticle-assembled microcapsules: an efficient and reusable catalyst. *Chem. Commun.* **2008**, *35*, 4165–4167.
(11) Caruso, F.; Caruso, R. A.; Mohwald, H. Nanoengineering of inorganic and hybrid hollow spheres by colloidal templating. *Science* **1998**, *282*(5391), 1111–1114.
(12) Caruso, F.; Caruso, R. A.; Mohwald, H. Production of hollow microspheres from nanostructured composite particles. *Chem. Mater.* **1999**, *11*(11), 3309–3314.
(13) Hah, H. J.; Kim, J. S.; Jeon, B. J.; Koo, S. M.; Lee, Y. E. Simple preparation of monodisperse hollow silica particles without using templates. *Chem. Commun.* **2003**, *14*, 1712–1713.
(14) Chen, M.; Wu, L. M.; Zhou, S. X.; You, B. A method for the fabrication of monodisperse hollow silica spheres. *Adv. Mater.* **2006**, *18*(6), 801−+.
(15) Lou, X. W.; Archer, L. A.; Yang, Z. C. Hollow Micro-/Nanostructures: Synthesis and Applications. *Adv. Mater.* **2008**, *20*(21), 3987–4019.

Published on Web 12/29/2010

Sol−gel chemistry has been applied to deposit an inorganic shell like silica on various templates like latex/inorganic sacrificial particles,[14,16−18] block copolymer or surfactant micelles[19−21] and microemulsions,[22−25] leading to inorganic-only capsules ranging from 30 nm to a few micrometers with good control over the shell thickness. This approach is comparatively more difficult to adapt to composite capsules, however. New scale-up-friendly methods are being developed, with notable ones involving polypeptide/polyamine-based biosilicification[26−30] and nanoparticle/polymer tandem assembly of nanoparticle-assembled capsules or "NACs".[31−38]

The synthesis of NACs proceeds through a simple two-step mixing process that involves ionic cross-linking of cationic polymers (like poly-L-lysine[31] or polyallylamine hydrochloride (PAH)[32]) and multivalent anions (like citrate or phosphate or EDTA) followed by the deposition of negatively charged 13 nm silica particles. The silica nanoparticles (NPs) form a shell around the polymer-anion aggregates, resulting in silica/polymer composite capsules (Figure 1). In addition to being a simple two-step mixing process, this method has the additional advantages of capsule size control, ease of encapsulation, mild pH and temperature processing conditions, the avoidance of a sacrificial core removal step, and compositional flexibility.[31,33−38]

Shell thickness of microcapsules has been shown to dictate the mechanical strength[39] and the permeability of the shell wall,[40] both of which need to be tuned for specific application needs.[41] NACs have shell thicknesses on the order of 100s of nm,[31,42] leading to structural robustness not found in LbL-assembled capsules (on the order of 10′s of nm).[12,39,40] In the case of LbL-assembled capsules formed through sequential deposition of oppositely charged colloidal species, the shell thickness is rationally controlled by the number of deposition steps. In comparison, there has been little attempt to control shell thickness of NACs at a finer scale because of an incomplete understanding of the shell-formation process.

In this work, it is shown that contacting the silica/polyamine NACs with silicic acid provides a reliable means to increase shell thickness. Silicic acid can be considered a metastable suspension of silicate oligomeric NPs that can interact electrostatically with the polyamines of the as-formed capsules. Through careful and detailed structural analysis, the shell appears to thicken in an inward direction as opposed to an outward direction expected for deposition on the shell exterior. Dye-release studies show a correlation between silicic acid concentration, resultant shell thickness, and diffusive release rate, providing insights into the shell formation and shell thickening processes.

2. Experimental Section

2.1. Materials. Polyallylamine hydrochloride (PAH, M.W. 56 kDa), tetramethylorthosilane (TMOS), sodium fluorescein

(16) Sadasivan, S.; Sukhorukov, G. B. Fabrication of hollow multifunctional spheres containing MCM-41 nanoparticles and magnetite nanoparticles using layer-by-layer method. *J. Colloid Interface Sci.* **2006**, *304*(2), 437–441.
(17) Zhou, J.; Wu, W.; Caruntu, D.; Yu, M. H.; Martin, A.; Chen, J. F.; O'Connor, C. J.; Zhou, W. L. Synthesis of porous magnetic hollow silica nanospheres for nanomedicine application. *J. Phys. Chem. C* **2007**, *111*(47), 17473–17477.
(18) Darbandi, M.; Thomann, R.; Nann, T. Hollow silica nanospheres: In situ, semi-in situ, and two-step synthesis. *Chem. Mater.* **2007**, *19*(7), 1700–1703.
(19) Feng, Z. G.; Li, Y. S.; Niu, D. C.; Li, L.; Zhao, W. R.; Chen, H. R.; Gao, J. H.; Ruan, M. L.; Shi, J. L. A facile route to hollow nanospheres of mesoporous silica with tunable size. *Chem. Commun.* **2008**, *23*, 2629–2631.
(20) Khanal, A.; Inoue, Y.; Yada, M.; Nakashima, K. Synthesis of silica hollow nanoparticles templated by polymeric micelle with core-shell-corona structure. *J. Am. Chem. Soc.* **2007**, *129*(6), 1534–+.
(21) Ras, R. H. A.; Kemell, M.; de Wit, J.; Ritala, M.; ten Brinke, G.; Leskela, M.; Ikkala, O. Hollow inorganic nanospheres and nanotubes with tunable wall thicknesses by atomic layer deposition on self-assembled polymeric templates. *Adv. Mater.* **2007**, *19*(1), 102–+.
(22) Fowler, C. E.; Khushalani, D.; Mann, S. Facile synthesis of hollow silica microspheres. *J. Mater. Chem.* **2001**, *11*(8), 1968–1971.
(23) Fujiwara, M.; Shiokawa, K.; Tanaka, Y.; Nakahara, Y. Preparation and formation mechanism of silica microcapsules (hollow sphere) by water/oil/water interfacial reaction. *Chem. Mater.* **2004**, *16*(25), 5420–5426.
(24) Wang, Q. B.; Yan, L.; Yan, H. Mechanism of a self-templating synthesis of monodispersed hollow silica nanospheres with tunable size and shell thickness. *Chem. Commun.* **2007**, *23*, 2339–2341.
(25) Bauer, C. A.; Robinson, D. B.; Simmons, B. A. Silica particle formation in confined environments via bioinspired polyamine catalysis at near-neutral pH. *Small* **2007**, *3*(1), 58–62.
(26) Cha, J. N.; Stucky, G. D.; Morse, D. E.; Deming, T. J. Biomimetic synthesis of ordered silica structures mediated by block copolypeptides. *Nature* **2000**, *403*(6767), 289–292.
(27) van Bommel, K. J. C.; Jung, J. H.; Shinkai, S. Poly(L-lysine) aggregates as templates for the formation of hollow silica spheres. *Adv. Mater.* **2001**, *13*(19), 1472–+.
(28) Sumper, M.; Lorenz, S.; Brunner, E. Biomimetic control of size in the polyamine-directed formation of silica nanospheres. *Angew. Chem., Int. Ed.* **2003**, *42*(42), 5192–5195.
(29) Jan, J. S.; Shantz, D. F. Biomimetic silica formation: Effect of block copolypeptide chemistry and solution conditions on silica nanostructure. *Adv. Mater.* **2007**, *19*(19), 2951–+.
(30) Belton, D. J.; Patwardhan, S. V.; Annenkov, V. V.; Danilovtseva, E. N.; Perry, C. C., From biosilicification to tailored materials: Optimizing hydrophobic domains and resistance to protonation of polyamines. *Proceedings of the National Academy of Sciences of the United States of America* **2008**, *105*, (16), 5963-5968.
(31) Rana, R. K.; Murthy, V. S.; Yu, J.; Wong, M. S. Nanoparticle self-assembly of hierarchically ordered microcapsule structures. *Adv. Mater.* **2005**, *17*(9), 1145–+.
(32) Murthy, V. S.; Rana, R. K.; Wong, M. S. Nanoparticle-assembled capsule synthesis: Formation of colloidal polyamine-salt intermediates. *J. Phys. Chem. B* **2006**, *110*(51), 25619–25627.
(33) Yu, J.; Murthy, V. S.; Rana, R. K.; Wong, M. S. Synthesis of nanoparticle-assembled tin oxide/polymer microcapsules. *Chem. Commun.* **2006**, *10*, 1097–1099.
(34) Yu, J.; Yaseen, M. A.; Anvari, B.; Wong, M. S. Synthesis of near-infrared-absorbing nanoparticle-assembled capsules. *Chem. Mater.* **2007**, *19*(6), 1277–1284.
(35) Kadali, S. B.; Soultanidis, N.; Wong, M. S. Assembling Colloidal Silica into Porous Hollow Microspheres. *Top. Catal.* **2008**, *49*(3−4), 251–258.
(36) Yaseen, M. A.; Yu, J.; Wong, M. S.; Anvari, B. Laser-induced heating of dextran-coated mesocapsules containing indocyanine green. *Biotechnol. Prog.* **2007**, *23*(6), 1431–1440.
(37) Yaseen, M. A.; Yu, J.; Wong, M. S.; Anvari, B. Stability assessment of indocyanine green within dextran-coated mesocapsules by absorbance spectroscopy. *J. Biomed. Opt.* **2007**, *12*, 6.
(38) Murthy, V. S.; Kadali, S. B.; Wong, M. S. Polyamine-Guided Synthesis of Anisotropic, Multicompartment Microparticles. *ACS Appl. Mater. Interfaces* **2009**, *1*(3), 590–596.
(39) Gao, C.; Donath, E.; Moya, S.; Dudnik, V.; Mohwald, H. Elasticity of hollow polyelectrolyte capsules prepared by the layer-by-layer technique. *Eur. Phys. J. E* **2001**, *5*(1), 21–27.
(40) Antipov, A. A.; Sukhorukov, G. B. Polyelectrolyte Multilayer Capsules As Vehicles with Tunable Permeability. *Adv. Colloid Interface Sci.* **2004**, *111*(1−2), 49–61.
(41) Bedard, M. F.; Munoz-Javier, A.; Mueller, R.; del Pino, P.; Fery, A.; Parak, W. J.; Skirtach, A. G.; Sukhorukov, G. B. On the mechanical stability of polymeric microcontainers functionalized with nanoparticles. *Soft Matter* **2009**, *5*(1), 148–155.
(42) Tavera, E. M.; Kadali, S. B.; Bagaria, H. G.; Liu, A. W.; Wong, M. S. Experimental and Modeling Analysis of Diffusive Release from Single-Shell Microcapsules. *AIChE J.* **2009**, *55*(11), 2950–2965.

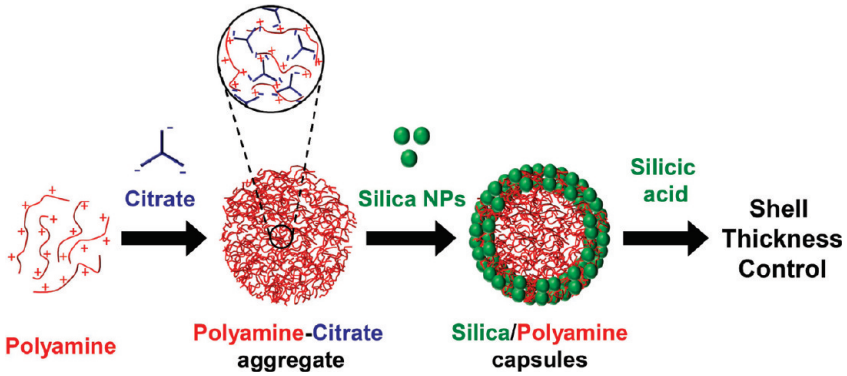

Figure 1. Schematic showing the synthesis of silica/polyamine capsules.

(Na-Flu), rhodamine B isothiocynate (RITC), and phosphate-buffered saline (PBS) were purchased from Sigma-Aldrich. Trisodium citrate dihydrate salt (citrate), NaCl, 1 N NaOH solution and 1 N HCl solution were obtained from Fisher Scientific. An aqueous colloidal suspension of silica NPs (Snowtex-O, 20.5 wt % silica, pH 3.5, ionic strength $I = 16.9$ mM)) was kindly provided by Nissan Chemicals. These NPs have a diameter of 13 ± 3 nm based on dynamic light scattering and a zeta potential value of -16 mV (Henry's equation) by electrophorectic measurements. POR 7 dialysis membrane (Spectrum Laboratories) with a molecular cutoff 2000 Da was used to prepare PAH-RITC conjugate following an earlier reported procedure.[32] Deionized water from a Barnstead Nanopure Diamond System (18.2 MΩ) was used to prepare all the solutions.

2.2. Synthesis of Silica/Polyamine NACs. The NACs were synthesized by first mixing PAH solution (14 mL, 5 mg/mL) and citrate solution (35 mL,14.2 mM) in a 250 mL beaker under gentle magnetic stirring (speed '4' of 0−10) for 10 s. The resulting suspension turned turbid instantly, indicating the formation of PAH-citrate aggregates.[32,35] After aging these aggregates for 30 min, 35 mL of 1.2 wt % silica NP sol (prepared by diluting 20.5% Snowtex-O with DI water, adjusted to pH 3.5 with 1 N HCl solution) was added. The resulting mixture was stirred vigorously (speed '7') for 10 min and aged for 2 h to form silica/polyamine NACs (Figure 1). For confocal imaging studies, 5% of PAH was replaced by PAH-RITC (with 1−2 Rhodamine B isothiocyanate molecules per PAH chain which contains ~750 amine groups).

2.3. Silicic Acid Treatment of NACs. To perform the silicic acid treatment, we added 0.43 mL of TMOS to a mixture of 34.22 mL of DI water and 0.35 mL of 0.1 N HCl, equivalent to a SiO_2 concentration of 0.5 wt %. Addition of TMOS to the acidic solution begins its hydrolysis and condensation[43] to yield oligomeric silicic acid clusters (or polysilicic acid, < 3 nm[44]) that are collectively referred to as "silicic acid". After 2 h of aging, the silica/polyamine NACs were resuspended by sonication and stirring. The silicic acid solution (35 mL), aged exactly for 30 min, was then added to the stirred NACs suspension, and the resulting mixture was stirred for another 30 min before withdrawing samples for analysis. For experiments involving silicic acid at a SiO_2 concentration of 0.1 wt %, the procedure was the same as above, except that 7 mL of the silicic acid solution was combined with 28 mL of DI water (pH 3.5 with HCl) just before adding to the stirred NACs suspension. For convenience, 0.1 and 0.5 wt % silicic acid-treated NACs will be referred to as NACs-(0.1%SA) and NACs(0.5%SA), respectively, and the untreated silica/polyamine NACs will be referred to as NACs(0%SA).

2.4. Dye Encapsulation and Permeability Study. Studies to gauge the relative permeability of silica/polyamine NACs and their silicic acid treated counterparts were carried out by encapsulating sodium fluorescein (Na-Flu), an anionic dye, and following its release kinetics. The Na-Flu encapsulation procedure is very similar to NAC synthesis. After combining the PAH and citrate solutions and aging this PAH-citrate mixture for 20 min, the Na-Flu dye solution (35 mL, 1 mg/mL) was added under gentle magnetic stirring for 10 s. The mixture was aged for another 10 min before the silica NP sol (35 mL, 1.2 wt %) was finally added. The resulting mixture was stirred vigorously (speed '7') for 10 min and aged for 2 h to form Na-Flu-encapsulated NACs(0%SA). These 2 h-aged NACs(0%SA) were then optionally treated with silicic acid, as described above.

Prior to performing the dye release experiments, NACs were cleaned to remove the excess Na-Flu. The cleaning was performed by dispersing the NACs (by sonication for 30 s and stirring), and separating them by centrifugation (Beckman-Coulter Allegra X-22 centrifuge at 6000 rpm for 7 min). All the supernatant was carefully removed and capsules redispersed in 30 mL of PBS buffer solution. Another round of centrifugation was performed to ensure complete removal of any superficial Na-Flu. The supernatant was carefully decanted and NACs were redispersed in 30 mL of PBS to begin the dye release studies. The NACs solution was quickly pippetted into 1.5 mL aliquots and placed on a rocking platform to ensure that the capsules do not settle. At various intervals, the aliquots were centrifuged for 5 min and UV−vis was performed on the supernatant to quantify the dye released. The amount of Na-Flu remaining in the capsules was also determined by breaking NACs with 0.1 N NaOH solution and performing UV−vis for mass balance verification.

2.5. Characterization Techniques. *Transmission Electron Microscopy* (*TEM*). Capsules were dried at 80 °C overnight and fixed using the PELCO Eponate 12 resin kit (from Ted Pella, Inc.). The formulation of the kit was chosen to obtain a resin of medium hardness. The cured resin was ultramicrotomed on a Leica Ultracut with a diamond knife to obtain ~200 nm slices. The slices were carefully collected onto carbon-coated copper grid and imaged with a JEOL 1230 high-contrast TEM operated at 80 kV.

Scanning Electron Microscopy (*SEM*). Capsules were dried on aluminum stubs from their DI water dispersions and sputter-coated

(43) Brinker, C. J.; Scherer, G. W. *Sol−Gel Science: The Physics and Chemistry of Sol-Gel Processing*; Academic Press: Boston, 1990; p 908.
(44) Bergna, H. E.; Roberts, W. O. *Colloidal silica: Fundamentals and Applications*; CRC Taylor & Francis: Boca Raton, FL, 2006; p 912.

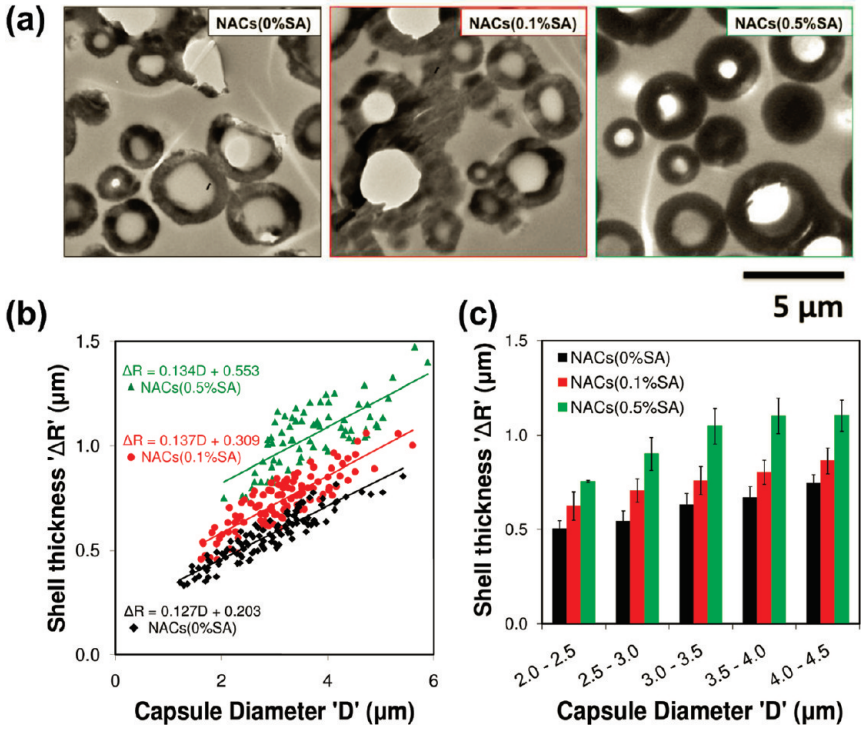

Figure 2. (a) Transmission electron microscopy (TEM) images of the microtomed sections of capsule samples and (b) corresponding capsule diameter and shell thickness measurements. (c) Histogram of shell thickness as a function of capsule diameter used in *t* test analysis to determine statistical significance.

with gold before imaging them on a FEI Quanta 400 field emission scanning electron microscope with the secondary electron detector. The electron gun was operated at 25 kV.

Confocal Microscopy. A Zeiss LSM 510 laser scanning confocal microscope utilizing a 63X Plan-Apochromat, (Numerical Aperture 1.4) was used to collect fluorescence image slices of the capsules. Samples for confocal microscopy were prepared by centrifuging 1 mL of NACs solution to remove the supernatant and dispersing them in DI water or 150 mM NaCl.

UV−Vis Spectroscopy. A Shimadzu 2401-PC UV−vis spectrophotometer and standard poly(methyl methacrylate) cuvettes with a path length of 1 cm were used.

Thermogravimetric Analysis. The weight loss-temperature profile for NACs was collected on a TA Instruments (SDT 2960 Simultaneous DSCTGA) thermogravimetric analyzer (TGA) with alumina pans. The temperature ramp rate was 5 °C/min and the air flow rate was 100 cm^3/min. The NACs were dried in an oven at 80 °C overnight prior to analysis.

Coulter Counter. Capsule diameter distribution was measured with a Beckman Multisizer 3 Coulter counter having an orifice diameter of 100 μm. The lower limit for measuring sizes for this orifice was 2 μm. The instrument calibration was verified by measuring 10 μm standard latex beads. The diameter of capsules was measured by diluting ~10 μL of the NACs PBS suspension in 20 mL of aqueous Isotone solution (composition: 7.93 g/L NaCl, 0.38 g/L Na_2EDTA, 0.40 g/L KCl, 0.19 g/L H_2NaPO_4, 1.95 g/L HNa_2PO_4, 0.30 g/L NaF; Beckman Coulter).

3. Results and Discussion

3.1. Shell-Thickness Determination. In total, three capsule samples were prepared and analyzed: as-synthesized capsules, NACs(0%SA); capsules treated with an amount of silicic acid, NACs(0.1%SA); and capsules treated with a higher silicic acid amount, NACs(0.5%SA). The thickness of the silica/polymer composite shell was measured through two techniques−transmission electron microscopy (TEM) and confocal microscopy. TEM image contrast being influenced by electron density (atomic number) of the sample is helpful in identifying the inorganic silica nanoparticles in the capsules. Confocal microscopy, on the other hand, uses fluorescence emission of the dye-conjugated polyallylamine hydrochloride (PAH) to image the organic component of the composite capsule.

TEM can successfully identify the internal structure of nanocapsules, but the contrast diminishes as the thickness of the material increases. For the three capsule samples being studied here, the micrometer size of the capsules significantly reduced the contrast making it difficult to identify the internal shell periphery for shell thickness measurement (see Figure S1 in the Supporting Information). In an effort to clearly identify the internal shell margin, microtomed sections of the resin-embedded capsules were imaged (Figure 2a).

The broadness in capsule size provided an opportunity to determine how shell thickness (ΔR) correlated to capsule diameters (D). Measurement of ~90 capsules for each of the three samples indicated shell thickness increased linearly with increasing diameters (Figure 2b). For a given diameter, the capsules generally had the following order for thickest shells: NACs(0.5%SA) > NACs(0.1%SA) > NACs(0%SA). Extrapolation of the thickness/diameter lines gave y-intercepts of 0.55, 0.31, and 0.20 μm, respectively, indicating the shells of NACs-(0.5%SA) and NACs(0.1%SA) were 0.35 and 0.11 μm thicker than the as-synthesized NACs.

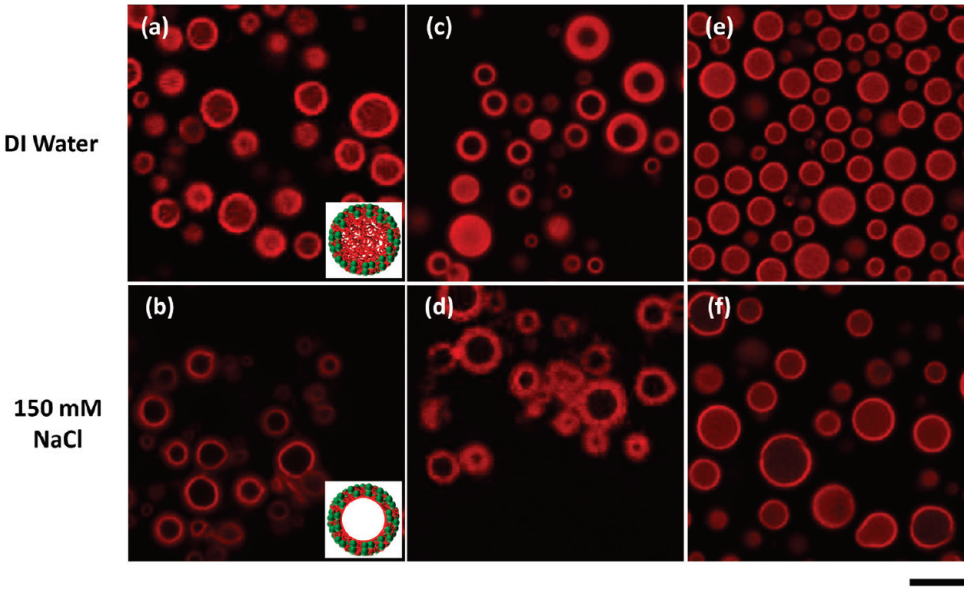

Figure 3. Confocal microscopy images of (a, b) NACs(0%SA), (c, d) NACs(0.1%SA), and (e, f) NACs(0.5%SA) dispersed in DI water (top row) or 150 mM NaCl solution (bottom row). Insets in a and b show the schematic structure of NACs in the respective image. Scale bar is 10 μm.

It is important to understand the source of scatter in the TEM data. The shell thickness ΔR and diameter D were presumed to be measured as if all the capsules were microtomed through its center. However, due to their wide size distribution and their random distribution within the epoxy resin, the microtome sectioning cannot be expected to run through the centers of each capsule exactly. Thus, there is some inherent error in the measured and true shell thickness and diameter, contributing to the data scatter. Shell thickness is more sensitive (therefore showing greater scatter in its measured values) than capsule diameter, based on geometrical arguments (see Figure S2 in the Supporting Information).

As the scatter caused some of the data points to overlap across samples, a *t* test was performed to verify that the samples were statistically different. The data from Figure 2b were split into bins of 0.5 μm from a *D* of 2 μm through 4.5 μm, as shown in Figure 2c. The average shell thickness for the three samples in each bin was then tested for statistical significance. A two sample *t* test at the 95% confidence level indicated p-values <0.013 (see Table S1 in the Supporting Information). Thus, in spite of the scatter, the difference in shell thicknesses between the NACs(0%SA)-NACs(0.1%SA) pair and NACs(0.1% SA)-NACs(0.5%SA) pair was real.

Confocal microscopy allowed for capsules to be analyzed while in suspension, and the low dye content of PAH-RITC (1−2 dye molecules per polymer chain) and a 5% amount of PAH-RITC mixed with the PAH ensured negligible interference of RITC in the formation of NACs.[31] For the as-synthesized polymer-filled capsules, the polymer was located in both the core (containing the PAH-citrate aggregate) and the shell (containing PAH and silica NPs). The fluorescence intensity difference between the core and the shell was not great enough for accurate thickness measurements, though (Figure 3a).

To address this imaging problem, the removal of the PAH-citrate core was sought. With the reasonable assumption that the electrostatic binding between PAH and silica NPs is greater than that between PAH and citrate because the NPs have many more negative binding sites than citrate anions, it was proposed that a salt solution could cause the disassembly of the PAH-citrate core and not cause the disassembly of the shell. Through a screening study, a NaCl solution with a concentration of 150 mM was successfully identified (Figure 3b). The loss in fluorescence in the core region of the now-hollow, water-containing capsules indicated dis-assembly of the PAH-citrate aggregates, which was verified in a separate DLS study (see Figure S3 in the Supporting Information).

For NAC samples treated with silicic acid, many of the capsules became hollow, while other capsules remained polymer-filled (Figure 3c). This hollowing behavior indicated the silicic acid nanoclusters had some capacity for dis-assembling the PAH-citrate core. All the capsules became hollow after placing them in a salt solution (Figure 3d), indicating that the PAH-citrate core was intact in many capsules after SA treatment and that the core could be dis-assembled in an electrolyte solution.

The salt solution treatment showed the NACs(0.1%SA) had visually thicker shells than NACs(0%SA). When treated with higher silicic acid concentration (NACs(0.5%SA)), none of the resulting capsules looked hollow (Figure 3e). None became hollow after placing them in a salt solution (Figure 3f), indicating that either the PAH-citrate core could not be disassembled (because of the silica newly deposited in the core interior), or the hollow core was too small to be visualized by confocal microscopy.

A statistical analysis of the shell thickness of NACs(0% SA) and NACs(0.1%SA) was performed by collecting intensity line profiles across the fluorescence image of capsules dispersed in 150 mM NaCl solution, and by measuring the average distance between the intensity

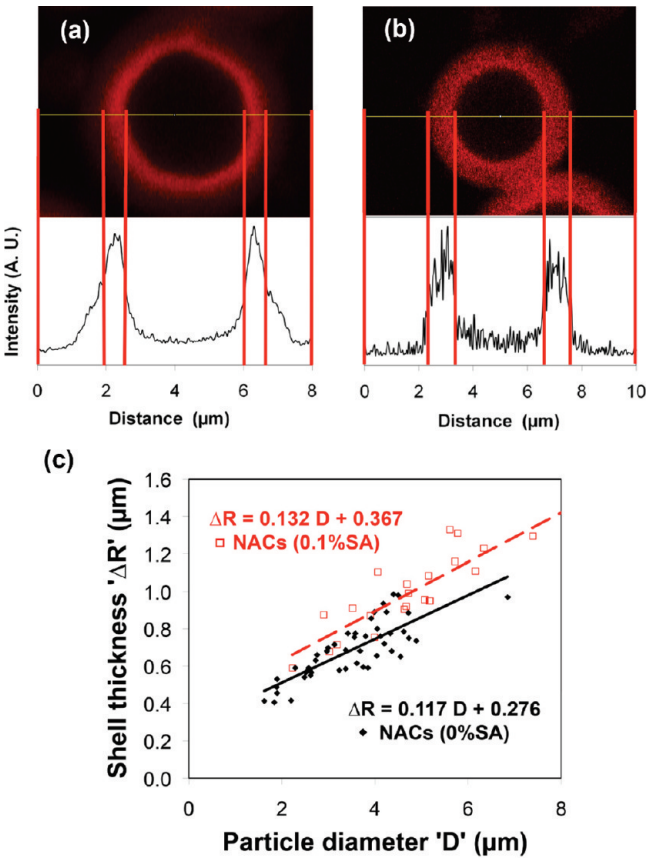

Figure 4. Intensity line profiles for (a) NACs(0%SA) and (b) NAC(0.1% SA). (c) Correlation between particle diameter and shell thickness based on intensity line profiles for NACs(0%SA) and NACs(0.1%SA).

midpoints on both sides of the left-hand and right-hand peaks (Figure 4a,b). The shell thickness was measured for ~30 capsules with various outer diameters, resulting in the correlations shown in Figure 4c. Thickness analysis of NACs(0.5%SA) was not performed, because the inner shell periphery could not be detected. In spite of the modest level of scatter in the data points, a linear correlation between capsule diameter and shell thickness could be ascertained for both capsule materials, which corroborated the TEM results. That the shell thickness depends on capsule diameter raises interesting questions about the kinetics and mechanism of shell thickening.

A comparison between correlations from confocal and TEM data showed the slopes of correlations to be similar. However, the y-intercepts (0.28 and 0.37 μm) were larger than the TEM-derived ones (0.20 and 0.31) for NACs(0% SA) and NACs(0.1%SA), respectively. For a given capsule diameter then, the shells are thicker in the wet state than in the dried state.

3.2. Capsule Diameter Measurements. Although TEM images of microtomed sections and confocal microscopy were useful in obtaining a shell thickness-capsule diameter correlation, capsule diameter themselves were more accurately determined by Coulter counter (in the wet state) and SEM (in the dry state). Coulter counter additionally provided the capsule counts as well.

The size curves obtained by Coulter counter closely resembled a log-normal distribution (Figure 5a), which is consistent with the polymer-salt aggregates growing via coalescence and with coalescence growth known to lead to log-normal particle size distributions.[32,45] The mean diameter of NACs(0%SA), NACs(0.1%SA), and NACs-(0.5%SA) were found to be 4.4, 4.3, and 4.5 μm, respectively. The corresponding standard deviations were 2.2, 2.0, and 2.1 μm. The capsule concentrations (after accounting for capsules below 2 μm based on log-normal fit) were found roughly to be the same for all samples, specifically 1.07×10^7, 1.04×10^7, and 1.12×10^7 capsules/mL, respectively. Silicic acid treatment was concluded to not change capsule size and did not skew the capsule size distribution.

Size distribution based on at least 600 capsules from SEM images (dry state) also resembled a log-normal distribution (Figure 5b, c). The mean diameters of NACs-(0%SA), NACs(0.1%SA), shrunk to 4.1 and 4.0 μm, respectively, with smaller standard deviations at 1.3 and 1.4 μm. This is consistent with our earlier study where capsules were larger in the wet state compared to the dried state also.[31] Interestingly, mean capsule diameter of NACs(0.5%SA) remained unchanged at 4.5 μm, suggesting that higher level of silicic acid rendered the capsule rigid, preventing shrinkage. These capsules too showed a smaller standard deviation at 1.6 μm. To gain confidence in the reported values, standard 3 μm Polybead beads were analyzed by SEM and Coutler counter. The mean size of the beads by the two techniques agreed very well each other, with Coulter counter showing slightly larger size distribution than SEM (see Figure S4 in the Supporting Information).

3.3. Proposed Shell-Thickening Process. The TEM results clearly show an increase in the shell thickness with increasing level of silicic acid treatment (Figure 2), which is also supported by the thicker polymer shell observed in confocal images after disassembly of the PAH-citrate core (Figure 3b, d, f). However, the fact that Coulter counter results indicate essentially no change in the average size, size distribution, or number counts of the capsules suggests that shell thickening by deposition of silicic acid took place in an inward direction. The Coulter counter results also indicate that any silicic acid that deposited on the exterior (which led to the smoother capsule surfaces observed via SEM; Figure 5c) did not measurably add to the capsule diameter and therefore did not increase wall thickness outward.

It was previously shown that silicic acid added to PAH-citrate aggregates yielded solid spheres, through the presumptive diffusion of the silicic acid nanoclusters and deposition within the aggregates.[31] This diffusion/deposition model is consistent with our observations of shell thickening without capsules increasing in diameter. The silicic acid oligomeric species diffuse through the permeable silica NP/PAH capsule wall, which subsequently deposit within the wall and on the inner shell wall surface (Figure 6). This shell-thickening mechanism suggests the

(45) de Lamaestre, R. E.; Bernas, H., Significance of lognormal nanocrystal size distributions. *Phys. Rev. B* **2006**, *73*, (12), -.

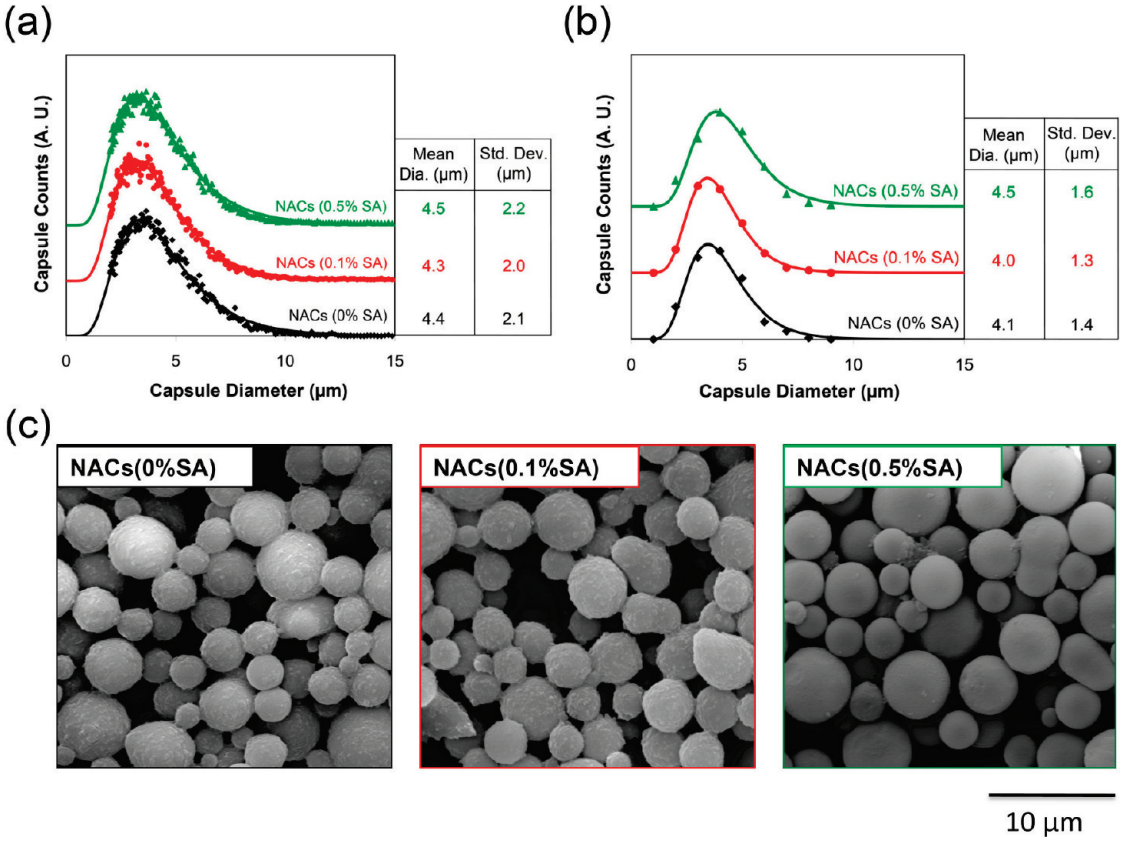

Figure 5. Capsule diameter distributions of NACs(0%SA), NACs(0.1%SA), and NACs(0.5%SA) from (a) Coulter counter measurements and (b) scanning electron microscopy (SEM), both fit to log-normal distributions. (c) SEM images of the three capsule samples.

interesting possibility of the shell having a density gradient in the radial direction, with the outer portion of the shell composed of silica NPs and PAH and the inner portion composed of PAH and silicic acid species.

3.4. Thermogravimetric Analysis. TGA was performed to assess the temperature-weight loss profile and the percentage inorganics present in each sample. As shown in Figure 7, the weight loss profile of the NACs(0%SA) was very similar to that observed in an earlier study.[35] The initial weight loss until ~220 °C resulted from both physically adsorbed and bound water. The weight loss from 220 °C through 600 °C occurred because of oxidation of the citrate anions and PAH (see Figure S5 in the Supporting Information) and the loss of water by condensation of surface silanol groups of the silica nanoparticles.[46,47] The final inorganic content of NACs(0%SA) was found to be 51%. Both NACs(0.1%SA) and NACs(0.5%SA) showed features very similar to those of NACs(0%SA) but with a decreased weight loss from 220 to 600 °C. There was a pronounced difference at ~260 °C, which we attribute to decreased citrate content caused by negatively charged silicic acid clusters diffusing into the silica/PAH NACs for shell thickening and displacing the negatively charged citrate ions. The higher inorganic content of NACs(0.1%SA) and NACs(0.5%SA) (57 and 61%, respectively) is consistent with this increase in silicic acid content and resultant thicker shells.

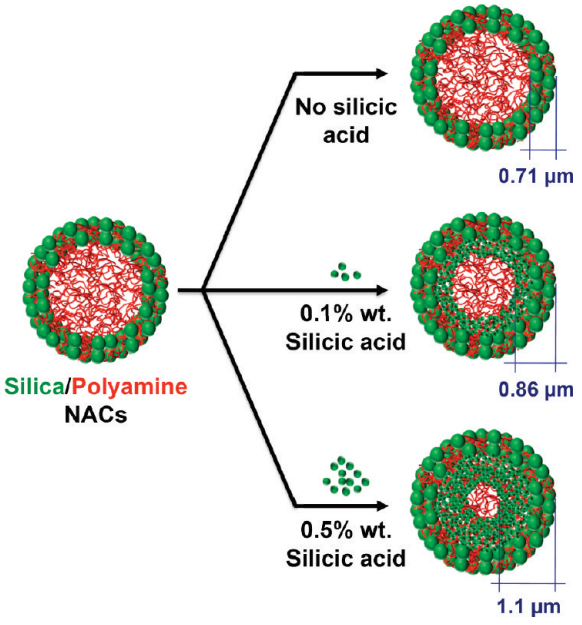

Figure 6. Schematic showing the shell-thickening process for 4 μm silica/polyamine NACs through silicic acid treatment. The shell thickness values come from the TEM correlations of Figure 2b.

3.5. Permeability Study. Dye-release studies were performed to evaluate the possible differences in permeability of the capsule shell wall by encapsulating sodium

(46) Jal, P.; Sudarshan, M.; Saha, A.; Patel, S.; Mishra, B. Synthesis and characterization of nanosilica prepared by precipitation method. *Colloids Sur., A* **2004**, *240*(1−3), 173–178.
(47) Mueller, R.; Kammler, H.; Wegner, K.; Pratsinis, S. OH surface density of SiO2 and TiO2 by thermogravimetric analysis. *Langmuir* **2003**, *19*(1), 160–165.

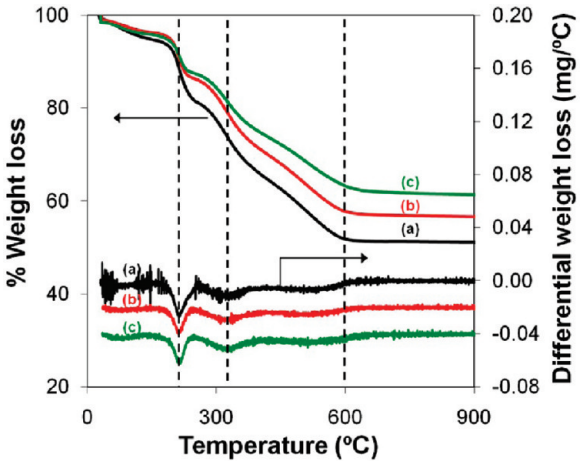

Figure 7. Thermogravimetric analysis of (a) NACs(0%SA), (b) NACs-(0.1%SA), and (c) NACs(0.5%SA).

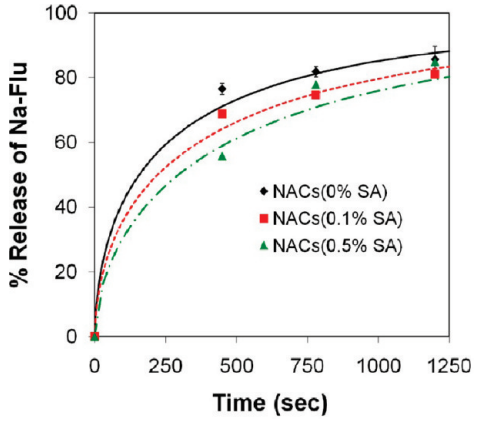

Figure 8. Fractional release of the encapsulated dye sodium fluorescein from NACs(0%SA), NACs(0.1%SA), and NACs(0.5%SA), shown with fitted curves based on single-shell microcapsule model.[42] Indicated error bars are from three independent experiments.

fluorescein (Na-Flu) in the capsules following an earlier reported procedure.[42] Successful deposition of silicic acid even in the presence of the Na-Flu was confirmed through TGA (see Figure S6 in the Supporting Information) and optical/fluorescence imaging (see Figure S7 in the Supporting Information) of Na-Flu encapsulated capsules. With the dye released into the supernatant and the amount remaining in the capsules determined separately to ensure all dye molecules were accounted (mass balance $>93\%$), the amounts of dye remaining in NACs(0%SA), NACs(0.1%SA), and NACs(0.5%SA) capsules were 0.7, 1, and 1.2 μg, respectively. The greater retention of dye with increasing shell thickness of NACs under the same processing conditions indicated the decreased permeability.

Quantitative values of permeability, defined as the ratio of the diffusion coefficient to the shell thickness, were obtained by fitting the release (Figure 8) to an analytical model that was recently developed by us,[42] using diffusion coefficient (of Na-Flu within the shell) as the sole adjustable parameter. The diffusion values for NACs (0%SA), NACs(0.1%SA) and NACs(0.5%SA) were determined to be 1.4×10^{-15}, 1.4×10^{-15}, and 1.1×10^{-15} m^2/s, respectively. On the basis of shell thickness obtained from Figure 2b, the corresponding permeabilities were calculated to be 2.0×10^{-9}, 1.5×10^{-9}, and 1.0×10^{-9} m/s. The small decrease in permeability (also seen as the rapid release for all three capsules, Figure 8) suggested the pores were still large enough after silicic acid treatment to not significantly slow down Na-Flu diffusive movement through the shell. Diffusion studies with probe molecules larger than Na-Flu (e.g., dextran[48]) may provide more detailed information on capsule porosity.

Conclusions

The present work demonstrates that the shell of silica/polymer hollow microspheres can be thickened by introducing silicic acid solutions of controlled concentrations to the microsphere suspension. TEM images of microtomed capsules and confocal images of the fluorescence-tagged version showed a linear relationship between shell thickness and capsule diameter in the dried and wet states, respectively, and showed silicic treatment led to thicker shells. SEM and Coulter counter measurements of capsules, in their respective dried and wet states, showed the capsules contracted slightly after drying and retained its log-normal size distribution. Silicic acid treatment did not increase capsule diameter, indicating that shell thickening took place in an inward direction. The increase in the inorganic content of capsules and the decreased dye-release permeability with increasing silicic acid concentration provided further evidence of silica deposition. This simple processing step for shell thickening should be readily extendable to other nanoparticle/polymer capsule formulations and to other charge-assembled structures.

Acknowledgment. We gratefully acknowledge funding support from the National Science Foundation (CBET-0652073), 3M (NTF Award), the Methodist Hospital Research Institute, and Sid W. Richardson Foundation (Institute of Biosciences and Bioengineering Medical Innovations Award Grant). We thank Mr. G. C. Kini for help with electron microscopy and useful discussions, Dr. E. M. Tavera for helpful discussions regarding the dye-release model, and Dr. J. Lomeda for help with TGA analysis. We are also very grateful to Mr. J. Summerville and Prof. M. Stern at Rice University for help with collection of ultramicrotome slices of capsules.

Supporting Information Available: TEM images of whole microcapsules (Figure S1), schematic showing geometric effects of slicing plane location on capsule shell thickness and diameter error (Figure S2), stability of PAH-citrate aggregates studied by dynamic light scattering (Figure S3), size analysis of 3 μm Polybead by SEM and Coulter counter (Figure S4), thermogravimetric analysis (TGA) of citrate and PAH (Figure S5), TGA of dye-encapsulated capsules (Figure S6), and optical/fluorescence microscopy images of dye-encapsulated capsules (PDF). This material is available free of charge via the Internet at http://pubs.acs.org/.

(48) Antipov, A. A.; Sukhorukov, G. B.; Leporatti, S.; Radtchenko, I. L.; Donath, E.; Mohwald, H. Polyelectrolyte multilayer capsule permeability control. *Colloids Surf., A* **2002**, *198*, 535–541.